

# Density Functional Study of Cubic to Rhombohedral Transition in $\alpha$ -AlF<sub>3</sub>

Yiing-Rei Chen<sup>1</sup>, Vasili Perebeinos<sup>2</sup>, and Philip B. Allen<sup>1,3</sup>

<sup>1</sup>*Department of Physics and Astronomy, State University of New York, Stony Brook, New York 11794-3800*

<sup>2</sup>*IBM Research Division, Thomas J. Watson Research Center, Yorktown Heights, New York 10598*

<sup>3</sup>*Department of Applied Physics and Applied Mathematics,  
and the Materials Research Science and Engineering Center,  
Columbia University, New York, New York 10027*

(Dated: May 5, 2019)

Under heating,  $\alpha$ -AlF<sub>3</sub> undergoes a structural phase transition from rhombohedral to cubic at temperature  $T$  around 730 K. The density functional method is used to examine the  $T=0$  energy surface in the structural parameter space, and finds the minimum in good agreement with the observed rhombohedral structure. The energy surface and electronic wave-functions at the minimum are then used to calculate properties including density of states,  $\Gamma$ -point phonon modes, and the dielectric function. The dipole formed at each fluorine ion in the low temperature phase is also calculated, and is used in a classical electrostatic picture to examine possible antiferroelectric aspects of this phase transition.

PACS numbers: 64.70.Kb, 71.20.-b, 77.80.Bh

## I. INTRODUCTION

The ionic insulator AlF<sub>3</sub> has a number of known polymorphs<sup>1,2</sup>, which all convert irreversibly to the stable  $\alpha$ -AlF<sub>3</sub> within the temperature range approximately 730 to 920 K. Recent interest in this material arises due to its catalytic activity for dismutation and halogen exchange reactions<sup>3</sup>.

Above its transition temperature (about 730 K)<sup>4</sup>,  $\alpha$ -AlF<sub>3</sub> has the cubic perovskite structure AMX<sub>3</sub>, with the A cations absent (or the ReO<sub>3</sub> structure.) Aluminum plays the role of the M cation, and is surrounded by an octahedron of corner-shared fluorine atoms. At low temperature, the structure becomes rhombohedral, and this symmetry lowering can be characterized as a rotation of the fluorine octahedron about one of the three-fold axis of the perovskite cubic cell (or the  $a^-a^-a^-$  system in Glazer's tilt system<sup>5</sup>). As every adjacent octahedron rotates in the opposite sense, the wave-vector of this distortion is  $(\pi, \pi, \pi)$ , and the unit cell becomes double the size of that in the cubic phase.

We study the  $\alpha$ -AlF<sub>3</sub> structure by using pseudopotentials, a plane-wave basis, and the LDA method. After being tested, the pseudopotentials are applied in bulk  $\alpha$ -AlF<sub>3</sub>. The total energy surface is examined in the structural parameter space where the cubic phase is compared with the rhombohedral phase found at the deepest nearby minimum of the energy surface.

## II. TESTING DIFFERENT PSEUDOPOTENTIALS

The Troullier and Martins method<sup>6</sup> is used to generate the pseudopotentials. Since there are different possibilities of choosing cut-off radii  $r_{cl}$ , as well as how many valence orbitals to include in the pseudopotentials, we test the pseudopotentials by doing LDA self-consistent

iterations for a crystal or molecule prototype and compare the results with FP-LAPW<sup>7</sup> all-electron calculations (full potential linearized augmented plane-wave<sup>8</sup>). This provides guidance on the choice of energy cut-off of the plane-wave basis, and also the choice of local potential, in the  $\alpha$ -AlF<sub>3</sub> calculation that follows. The results of these tests are shown in Table I and Table II, for aluminum and fluorine separately. For the Ceperley-Alder exchange-correlation energy<sup>9</sup>, the Vosko-Wilk-Nusair<sup>10</sup> parametrization is used.

The test of the aluminum pseudopotential is performed in bulk Al metal, not only the observed *fcc* structure, but also the *sc* and *bcc* structures, where comparison can still be made between the all-electron method and LDA. The results show that the pseudopotential for the Al<sup>3+</sup> ion should be capable of describing the unoccupied *3d* orbital. Otherwise, even the large  $r_{cl}$  ( $l = 0, 1$  for *s* and *p* orbitals) needed to fix the lattice constant in the *fcc* aluminum are insufficient to remove the  $r_{cl}$ -dependence of the lattice constant and bulk modulus. Due to the more attractive nature of the *d* pseudopotential, including the *3d* orbital reduces the dependence of these two quantities on  $r_{cl}$  and the choice of local potential, and improves the agreement with the all-electron results. Better agreement is also seen in comparisons for *sc* and *bcc* structures of Al metal.

The fluorine pseudopotential is tested for the F<sub>2</sub> molecule. Unlike the low plane-wave cut-off needed for aluminum (less than 40 Rydberg), more than 90 Rydberg is needed in the F<sub>2</sub> molecule. For bulk Al metal we use a k-point mesh of  $12 \times 12 \times 12$  that contains 56 special k-points, while for F<sub>2</sub> we do a one k-point calculation.

Results in the following sections are calculated using pseudopotentials (Al<sup>†</sup>, F<sup>†</sup>) as shown in the captions of the Tables. This set of pseudopotentials gives the lattice constant ( $a = 5.02\text{\AA}$ ), and bulk modulus ( $B = 146.6$  GPa) of cubic  $\alpha$ -AlF<sub>3</sub> in good agreement with all-electron results ( $a = 5.043\text{\AA}$ ,  $B = 150$  GPa.)

TABLE I: Aluminum pseudopotential tests on bulk Al. The first column shows the cut-off radii in units of Bohr radius ( $a_0$ ) for the valence orbitals ( $l=0,1,2$ ). Tests with  $r_{c2}$  omitted do not include the  $d$  orbital. The following columns show the use of core correction, the choice of local potential, lattice constant, bulk modulus and the total energy per atom with respect to the  $fcc$  structure. Values are shown in atomic units ( $e$  = electron charge,  $a_0$  = Bohr radius.)  $\Delta E$  is defined to be zero for the  $fcc$  structure, while the total energy differences between  $fcc$  and other structures can be compared with all-electron results. The pseudopotential with a  $\dagger$  is chosen for the calculations of  $\alpha$ -AlF<sub>3</sub>.

$r_{c0}/r_{c1}/r_{c2}$ ( $a_0$ )	core corr.	local	lattice const.( $a_0$ )	B ( $\times 10^{-3} e^2/a_0^4$ )	$\Delta E$ ( $e^2/a_0$ )
<i>fcc</i> structure					
2.2/2.5/—	yes	<i>s</i>	7.738	2.487	0
2.4/2.5/—	yes	<i>s</i>	7.712	2.524	0
2.6/2.6/—	yes	<i>s</i>	7.672	2.607	0
1.9/2.4/2.7	yes	<i>d</i>	7.507	2.873	0
1.8/2.2/2.7	yes	<i>s</i>	7.500	2.850	0
1.8/2.2/2.7	yes	<i>p</i>	7.516	2.896	0
1.8/2.2/2.7	yes	<i>d</i>	7.507	2.873	0
1.8/2.2/2.6	yes	<i>d</i>	7.505	2.934	0
2.6/2.6/2.6 <sup>†</sup>	no	<i>d</i>	7.481	2.865	0
all-electron	—	—	7.536	2.905	0
experiment	—	—	7.650	2.579	—
<i>sc</i> structure					
1.9/2.4/2.7	yes	<i>d</i>	5.063	2.176	0.01431
1.8/2.2/2.7	yes	<i>s</i>	5.061	2.170	0.01451
1.8/2.2/2.7	yes	<i>p</i>	5.069	2.195	0.01425
1.8/2.2/2.7	yes	<i>d</i>	5.063	2.177	0.01431
1.8/2.2/2.6	yes	<i>d</i>	5.062	2.175	0.01436
2.6/2.6/2.6 <sup>†</sup>	no	<i>d</i>	5.050	2.072	0.01462
all-electron	—	—	5.065	2.096	0.01449
<i>bcc</i> structure					
1.9/2.4/2.7	yes	<i>d</i>	6.015	2.546	0.00368
1.8/2.2/2.7	yes	<i>s</i>	6.009	2.534	0.00374
1.8/2.2/2.7	yes	<i>p</i>	6.023	2.581	0.00368
1.8/2.2/2.7	yes	<i>d</i>	6.015	2.542	0.00368
1.8/2.2/2.6	yes	<i>d</i>	6.014	2.538	0.00370
2.6/2.6/2.6 <sup>†</sup>	no	<i>d</i>	5.992	2.472	0.00380
all-electron	—	—	6.027	2.525	0.00414

### III. RESULTS FROM LDA

#### A. k-point Test and Density of States

A k-point mesh of  $3 \times 3 \times 3$  is used for the Brillouin zone summation for  $\alpha$ -AlF<sub>3</sub>. This is tested for cubic  $\alpha$ -AlF<sub>3</sub>, where a finer mesh of  $4 \times 4 \times 4$  gives a barely different energy *vs* plane wave cut-off curve, with energy uncertainty less than 1 meV. This mesh gives six special k-points after symmetrization (according to the point group  $D_{3d}$  of the

TABLE II: Fluorine pseudopotential tests on F<sub>2</sub> molecule. The last column indicates the plane-wave cut-off needed to obtain the convergent result. The pseudopotential with a  $\dagger$  is chosen for the calculations of  $\alpha$ -AlF<sub>3</sub>.

$r_{c0}/r_{c1}$ ( $a_0$ )	core corr.	local	bond ( $a_0$ )	force const.( $e^2/a_0^3$ )	cut-off (Ryd.)
1.4/1.6	no	<i>p</i>	2.780	0.370	90
1.4/1.45	yes	<i>p</i>	2.710	0.408	90
1.3/1.3	yes	<i>s</i>	2.599	0.384	over 100
1.3/1.3 <sup>†</sup>	no	<i>s</i>	2.603	0.376	90
1.2/1.2	yes	<i>s</i>	2.617	0.387	over 100
all-electron	—	—	2.632	0.376	—
experiment	—	—	2.669	0.302	—

crystal), over which we include at least 36 states in the truncated Hamiltonian diagonalization processes. Since in the rhombohedral unit cell of  $\alpha$ -AlF<sub>3</sub> we consider the 48 valence electrons from aluminum  $3s^23p^1$  and fluorine  $2s^22p^5$ , these electrons will occupy the 24 lowest lying bands. A test including more states, 48 states for example, shows that in the process of iterative diagonalization, using 36 states gives convergent answers for the eigenvalues of the lowest 24 bands. Thus we include 36 states in the calculation of the minimum on the energy surface. To make the density of states plot, we include 50 states to better describe the empty states from aluminum orbitals. As shown in Fig. 1, LDA gives an insulator band-gap of 8 eV. We choose 90 Rydberg to be the energy cut-off for the plane-wave basis. This choice gives the same energy difference between the two structures as that from the choice of 140 Rydberg (with error within  $1 \sim 2$  meV. The two structures are the cubic and the rhombohedral structure at the minimum.)

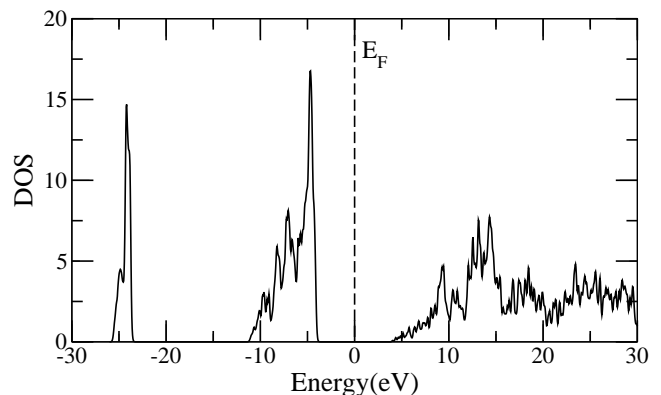


FIG. 1: Density of states plot of  $\alpha$ -AlF<sub>3</sub> in the rhombohedral ground state, using pseudopotential (Al<sup>†</sup>, F<sup>†</sup>). The rhombohedral ground state has unit cell edge  $4.76 \text{ \AA}$ ,  $\theta=57.5^\circ$  and  $\delta=0.098$ . This calculation includes 50 states and uses a k-point mesh  $6 \times 6 \times 6$ . The temperature broadening is 54 meV.

## B. Crystal Structure

We use LDA to search for the ground state in the rhombohedral symmetry class  $R\bar{3}C$  seen experimentally in  $\alpha$ - $\text{AlF}_3$ <sup>4</sup>. There are three free parameters: (1) the lattice constant  $a$ , (2) the angle  $\theta$  between any two of the rhombohedral lattice vectors, and (3) the inner parameter  $\delta$ , which describes the bending of the Al-F-Al bond. To describe these three parameters, we first start from the cubic structure with lattice vectors  $(2b, 0, 0)$ ,  $(0, 2b, 0)$  and  $(0, 0, 2b)$ , where  $b$  is the Al-F bond length. A rhombohedral unit cell is formed by picking new lattice vectors  $\vec{a}_1 = (0, 2b, 2b)$ ,  $\vec{a}_2 = (2b, 0, 2b)$ , and  $\vec{a}_3 = (2b, 2b, 0)$ . The angle  $\theta$  defined as  $\theta = \cos^{-1}(\vec{a}_1 \cdot \vec{a}_2 / |\vec{a}_1||\vec{a}_2|)$  is  $60^\circ$  in this case. This new cell is then elongated along the [111] direction. Consequently, the strains  $\epsilon_{23} = \epsilon_{31} = \epsilon_{12}$  become nonzero, and  $\theta \neq 60^\circ$ . Viewed from the [111] direction, in the aluminum plane the ions form a hexagonal pattern, and the nearest Al-Al distance on this (111) plane is the lattice constant  $a$ . This rhombohedral structure can also be described in a hexagonal setting, with the following  $c/a$  ratio

$$\frac{c}{a} = \sqrt{\left(\frac{3}{2}\right) \left(\frac{1+2\cos\theta}{1-\cos\theta}\right)} \quad (1)$$

The cell shape and cell volume  $V$  are determined by  $a$  and  $c/a$ :

$$V = \frac{a^3}{2\sqrt{2}} \sqrt{\frac{1+2\cos\theta}{1-\cos\theta}} = \frac{a^2 c}{2\sqrt{3}}, \quad (2)$$

while the relation between the lattice constant  $a$  and the length of the rhombohedral lattice vectors is:

$$a/|\vec{a}_1| = \sqrt{2(1-\cos\theta)} \quad (3)$$

There are two aluminum ions and six fluorine ions in each rhombohedral unit cell. The fluorine ions sit at the 6e sites  $((x, \bar{x} + \frac{1}{2}, \frac{1}{4}), (x, x + \frac{1}{2}, \frac{3}{4}), \text{etc.})$ , and  $\delta=x-0.75$  is the deviation from  $x=0.75$  where the Al-F-Al bond angle is strictly  $180^\circ$ . The distortion caused by  $\delta$  alone defines the octahedron rotation angle  $\omega$  about the [111] axis:

$$\tan\omega = 2\sqrt{3}\delta, \quad (4)$$

On the other hand, the  $c/a$  ratio and the  $\omega$  have the following relation:

$$\frac{c}{\sqrt{6}a} = \frac{1+\zeta}{\cos\omega}, \quad (5)$$

where  $\zeta$  describes the flattening ( $\zeta < 0$ ) and elongation ( $\zeta > 0$ ) of the octahedron along [111].

We first assume cubic symmetry by fixing  $\theta = 60^\circ$  and  $\delta = 0$ . LDA gives the lattice constant  $a = a^* = 5.02\text{\AA}$  for the cubic phase. With the lattice constant kept fixed at the value  $a = a^*$ ,  $\delta$  is then relaxed to give minimum energy at  $(a, \theta, \delta) = (a^*, 60^\circ, \pm 0.04)$ . As shown in Fig.

2, the relaxation of  $\delta$  finds minima at  $\delta = \pm 0.04$  and a maximum at  $\delta = 0$ , with an energy difference of 14.4 meV, showing that in our  $T=0$  energy surface study, the unbent Al-F-Al bond, and therefore the strictly cubic structure, is not a metastable solution.

The three parameters are then relaxed in turn to approach the deepest nearby minimum. In fact, in the parameter space, there is a path that keeps the fluorine octahedra rigid and leads to the region near the overall minimum. A Rigid octahedron means that the Al-F bonds are fixed at the bond length found by LDA in the cubic phase

$$b = \frac{a^*}{2\sqrt{2}} = \frac{a}{2\sqrt{2}\cos\omega} \quad (6)$$

and that the angles between neighboring Al-F bonds are always 90 degrees ( $\zeta = 0$ ). With these two restrictions, only one parameter  $\delta$  remains and defines the rigid octahedron path. The energy along this path is also shown in Fig. 2. The overall minimum locates not far from the minimum on this path. It has an Al-F bond length only 0.3% longer, a pretty small octahedron elongation factor  $\zeta = 0.25\%$ , and the total energy 93 meV lower than the cubic phase. Table III shows the comparisons between LDA and experimental data<sup>4</sup>. While no  $T = 0$  experimental numbers are available, one can only make reasonable comparisons for the deviation of bond length and  $\zeta$ . The rhombohedral phase observed in the experiment has an Al-F bond length 0.43% longer than the value observed in the cubic phase, and  $\zeta = -0.102\%$  (meaning the octahedron is slightly flattened.) This indicates that both the LDA and the experimentally found rhombohedral phases are close to the rigid octahedron path.

TABLE III: The structure parameters found by LDA are compared with experimental values<sup>4</sup> here for different phases. The total energy (per two formulas of  $\text{AlF}_3$ ) difference between the two phases is also shown here, where the total energy of the cubic phase is set to zero. The values for the rhombohedral phase are calculated at the minimum of the energy surface.

	lattice const.( $\text{\AA}$ )	$\theta$ ( $^\circ$ )	$\delta$	$\Delta E$ (meV)
psp( $\text{Al}^\dagger, \text{F}^\dagger$ ) rhom	4.76	57.5	0.098	-93
experiment (LT)	4.9382	58.82	0.0691	—
psp( $\text{Al}^\dagger, \text{F}^\dagger$ ) cubic	5.02	60.0	0.0	—
experiment (HT)	5.0549	59.94	0.0129	—

## C. Phonon Modes

Previous workers<sup>11</sup> investigated the phonon spectrum of the cubic phase using the generalized Gordon-Kim method<sup>12</sup>. Density functional theory was applied to construct the charge distribution and polarizability of ion.

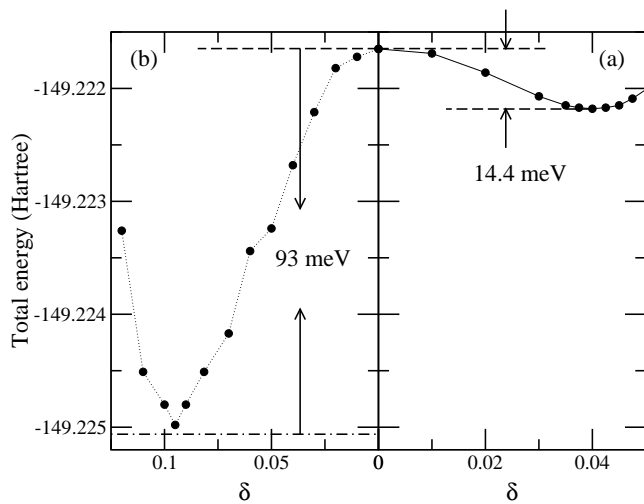


FIG. 2: The relaxation of  $\delta$  from the cubic structure is shown in plot (a). The curve of total energy (per two formulas of  $\text{AlF}_3$ ) vs  $\delta$  at  $\theta = 60.0^\circ$  and  $a = 5.02\text{\AA}$  shows that the cubic phase is sitting at an energy maximum. In (b), the curve follows the rigid-octahedron path, and leads to the region near the overall minimum in the parameter space. The dotted-dashed line shows the energy of the overall minimum.

An approximate crystal energy is then calculated from the ion results, and is used to examine the crystal lattice dynamics. However they did not find an instability of the cubic phase, which is contradictory to the experiment. Here we use full LDA to examine the energy surface around the rhombohedral minimum, and extract the soft phonon modes directly. The rhombohedral minimum described in the previous section, and the dipole aspect discussed in Sec. IV, both show the instability of the cubic phase.

At the  $\Gamma$  point of the rhombohedral phase, the irreducible representations are those of the point group  $D_{3d}$  (note that the space group of the rhombohedral phase is  $R\bar{3}C$ , which is nonsymmorphic.) Among the 12  $\Gamma$  point modes provided by the fluorines, namely,  $A_{1g} \oplus 2A_{2g} \oplus 3E_g \oplus A_{1u} \oplus 2A_u \oplus 3E_u$ , the four modes  $A_{1g} \oplus 3E_g$  are Raman active. Viewed from the cubic phase, the octahedron rotation that governs the structural transition is the  $R_5$  mode (in Kovalev labelling) at the zone boundary  $(\pi, \pi, \pi)^{13}$ . After distortion, the  $R_5$  mode gives rise to the zone-center  $A_{1g}$  mode and one of the three  $E_g$  modes. Raman experiments<sup>13,14</sup> showed that the  $A_{1g}$  and one  $E_g$  are the soft phonon modes below transition. The  $A_{1g}$  is the Al-F-Al bond angle bending mode. Using the fluorine atomic mass, and the energy vs  $\delta$  curve, the  $A_{1g}$  frequency is calculated to be  $205\text{ cm}^{-1}$ . We also calculate the other restoring coefficients of the three  $E_g$  modes, and the two Raman-inactive  $A_{2g}$  modes. Their frequencies are listed in Table. IV.

TABLE IV: Some of the  $\Gamma$  point phonon modes frequencies calculated by LDA. direct comparison with experiments are not available since previous observations are done at RT and above. However, in the experiment it is found that the two high energy  $E_g$  modes only weakly depend on temperature. A crude extrapolation using  $\omega^2 = A(T - T_c)$  (from Curie-Weiss law and Lyddane-Sachs-Teller relation) and the RT experimental data<sup>13</sup> gives the frequency values at  $T = 0$ .

	$A_{1g}$	$E_g$	$E_g$	$E_g$
LDA	205	182	350	487
experiment(RT)	158	98	383	481
extrapolation	190	118	388	481
	$A_{2g}$	$A_{2g}$		
LDA	361	691		

#### D. Dielectric Function

The electronic part of the dielectric tensor  $\epsilon(\mathbf{q} = 0, \omega)$  is also calculated.  $\epsilon_{xx} = \epsilon_{yy} \neq \epsilon_{zz}$  is expected since we have chosen lattice vectors such that  $\hat{x}$  and  $\hat{y}$  are perpendicular to the three-fold axis. The imaginary part of the dielectric function can be directly obtained by calculating all direct inter-band transitions<sup>15</sup>:

$$\epsilon_2(\omega) = \left(\frac{2\pi e}{m\omega}\right)^2 \sum_k \sum_{m,n} |\langle \psi_{n,k} | \vec{p} | \psi_{m,k} \rangle|^2 f_n(1 - f_m) \times \delta(E_m - E_n - \hbar\omega), \quad (7)$$

where  $\vec{p}$  is the momentum operator, and  $k$  runs through all  $k$ -points in the Brillouin zone allowed in a unit volume. The band indices are  $m$  and  $n$ ,  $f_{n,k}$  and  $f_{m,k}$  are the occupation number of the  $n^{\text{th}}$  and  $m^{\text{th}}$  states at the  $k^{\text{th}}$   $k$ -point. The real part of dielectric function is obtained using the Kramers-Kronig relation. The result at  $T=0$  is given in Fig. 3, but we do not know of any experiment to compare with. However this calculation does neglect the non-local potential effect<sup>16</sup> and the local field effect<sup>17</sup>, and follows the pseudo-wave-functions that are smoothed in the ion core regions.

#### IV. INNER PARAMETER $\delta$ AND DIPOLE FORMATION

The formation of a dipole plays an important role in the energy difference between the two  $\alpha$ - $\text{AlF}_3$  structures. When the inner parameter  $\delta$  is non-zero, each fluorine atom develops a dipole (Aluminum atoms sit on inversion centers and therefore cannot have dipoles). Starting from the cubic structure, the distortion from  $\delta$  alone defines the octahedron rotation angle  $\omega$  about the  $[111]$  axis (see Eq. 4) and already lowers the symmetry to  $R\bar{3}C$ . The parameter  $\delta$  is irrelevant to the  $c/a$  ratio, but it does flatten the octahedron (see Eq. 5). It also elongates the

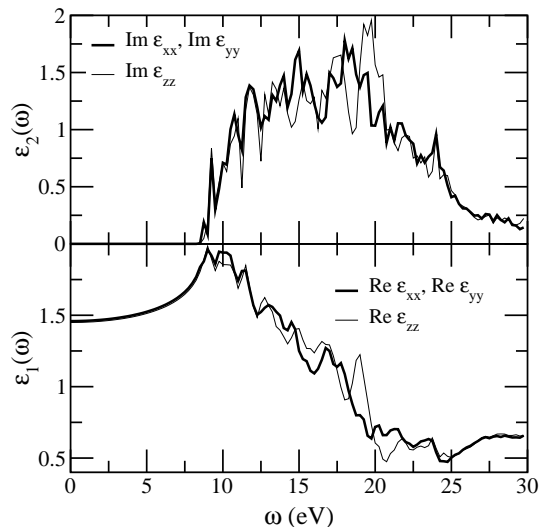


FIG. 3: Plots of dielectric functions. This calculation includes 50 states and uses a k-point mesh  $6 \times 6 \times 6$ .

Al-F bond length, and introduces a polarization to each fluorine. The energy gain from the fluorine dipole-dipole interaction drives the structure off-cubic. This is shown in Fig. 2, where the cubic structure is found to be not a metastable solution.

A naive picture of ionic solids has spherical electron charge clouds of total charge  $Q_i$  around the  $i^{\text{th}}$  ion. In reality, charge clouds are distorted. For example, in high T cubic  $\alpha$ -AlF<sub>3</sub>, the F ions are noticeably prolate when examined in a (100)-plane charge contour calculation<sup>18</sup>. This distortion is still evident in the low T rhombohedral phase, as shown in Fig. 4. The value of the charge  $Q_i$ , on the other hand, is not uniquely definable. By creating a sphere centered at each fluorine atom, with a radius that only allows neighboring spheres in the rhombohedral phase to touch each other at one point, we define a volume to examine the charge and the dipole moment of the fluorine. In the cubic phase, such a sphere contains charge  $-0.675|e|$ , while it contains  $-0.68|e|$  in the rhombohedral phase (with a slightly different radius.) Using the same sphere, we compute the local induced dipole moment  $\mathbf{p}_{\text{ind}}$  of the fluorine ion (which also has no unique definition<sup>19</sup>.) As expected from symmetry,  $p_{\text{ind}} = 0$  in the cubic phase, whereas  $p_{\text{ind}} = 0.103|e|\text{\AA}$  in the rhombohedral phase, pointing from the fluorine position of the unbent Al-F-Al bond towards the actual distorted fluorine position. Note that the displacive dipole is  $p_{\text{dis}} = 0.315|e|\text{\AA}$ , defined by the fluorine charge  $-0.675|e|$  and the displacement  $0.467\text{\AA}$  of the fluorine ion when the Al-F-Al bonds bend. By symmetry, the other fluorine sitting at the opposite side of the octahedron has its dipole pointing exactly in the opposite direction. Therefore the material could be called antiferroelectric<sup>20</sup>.

The dipoles and charges can as well be determined by doing integration in one of the equivalent polyhedra that surround the F<sup>-</sup> ions and partition the whole space (the

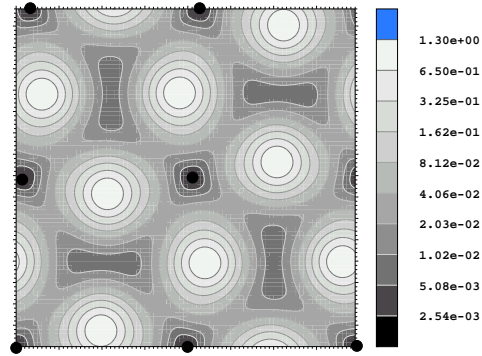


FIG. 4: Charge density plot of the rhombohedral phase on a (100) plane. The [100] direction is ill-defined since it is inherited from the cubic phase, but the plane shown here does contain the aluminum ions (labelled in solid dots) that form the (100) plane in the cubic phase. The fluorine ions are slightly off the plane shown here, and display clearly a prolate charge distribution.

Al<sup>3+</sup>'s sit on shared vertices of the F<sup>-</sup> polyhedra.) In this way, the ions are charged as Al<sup>3+</sup> and F<sup>-</sup>, while  $p_{\text{ind}} = 0.0963|e|\text{\AA}$  and  $p_{\text{dis}} = 0.467|e|\text{\AA}$ .

It is worthwhile to see if a simplified picture with these numbers helps to understand the energy. In LDA, the energy includes the exact electrostatic or Hartree energy from the electron charge clouds, as well as other quantum effects (energy of delocalization, exchange and correlation.) Purely classical electrostatic models (plus hard core repulsion), on the other hand, provide a simple but useful view. We shall see how much classical electrostatic energy comes from the charge and if this helps to explain the stability of the structural deformation.

In a simplified picture where only electrostatic energy and dipole formation energy ( $E_1$  in Eq. 8, where  $\alpha = 0.858\text{\AA}^{321}$ ) are considered, the total energy is

$$\begin{aligned}
 E &= E_1 + E_2 + E_3 + E_4 \\
 &= \sum_i \frac{\mathbf{p}_i^2}{2\alpha} + \sum_i \sum_{j<i} \frac{Z_i Z_j}{r_{ij}} + \sum_i \sum_{j<i} \frac{Z_i (\mathbf{p}_j \cdot \mathbf{r}_{ij})}{r_{ij}^3} \\
 &\quad + \sum_i \sum_{j<i} \frac{\mathbf{p}_i \cdot \mathbf{p}_j - 3(\hat{\mathbf{r}}_{ij} \cdot \mathbf{p}_i)(\hat{\mathbf{r}}_{ij} \cdot \mathbf{p}_j)}{r_{ij}^3}. \quad (8)
 \end{aligned}$$

This form leaves out the quantum effects and the effect from covalent bond angle. We find that  $E_2$ , which is purely ionic electrostatic (including displacive dipoles), is less negative in the rhombohedral structure than in the cubic structure (i.e., if the same ion charge assignment is considered in both cases.) However, when the induced-dipole-related terms ( $E_1 + E_3 + E_4$ ) are also considered, the energy is lowered. By assuming point charges and point dipoles, we use the results from the polyhedron method to illustrate this picture:  $E_2$  per two AlF<sub>3</sub> formulas in the rhombohedral phase is 1 eV higher than that

in the cubic phase; but  $E_3$  and  $E_4$  bring the energy  $E$  down, with the cost of  $E_1$ , to 0.97 eV lower than the cubic phase (which has only  $E_2$ .) This suggests that the effect of induced dipoles is more than enough to compensate the energy loss from the structural distortion.

## V. CONCLUSION

We report an LDA study of bulk  $\alpha$ -AlF<sub>3</sub>. By examining the  $T=0$  energy surface for structures of the phases on both sides of the transition, we find the structural parameters to agree with previous experiments, and the cubic phase not to be a metastable solution. Using the result of LDA, the density of states plot and the dielectric function are provided. At the  $\Gamma$ -point, the predicted  $A_{1g}$  soft phonon mode and  $E_g$  modes are compared with previous Raman experiment, while two other  $A_{2g}$  modes are predicted. We look at the charge and dipole moment

at each fluorine ion, and use these quantities to calculate the classical electrostatic energy. In the antiferroelectric distortion which accompanies the structural transition, a classical calculation shows that the electrostatic energy gain from dipoles is more than enough to compensate the energy loss from the ion-array deformation.

## Acknowledgments

We thank C. Grey and S. Chaudhuri for suggesting the project and for helpful discussions. The LDA code (BEST) and the FT-LAPW code is provided by Brookhaven National Laboratory. Work at Stony Brook was supported in part by NSF grant no. DMR-0089492. Work at Columbia was supported in part by the MR-SEC Program of the National Science Foundation under Award Number DMR-0213574.

- 
- <sup>1</sup> N. Herron, D. L. Thorn, R. L. Harlow, G. A. Jones, J. B. Parise, J. A. Fernandez-Baca, and T. Vogt, *Chem. Mater.* **7**, 75 (1995).
- <sup>2</sup> C. Alonso, A. Morato, F. Medina, F. Guirado, Y. Cesteros, P. Salagre, and J. E. Sueiras, *Chem. Mater.* **12**, 1148 (2000).
- <sup>3</sup> E. Kemnitz and L. E. Manzer, *Prog. Solid State Chem.*, **26** 97 (1998).
- <sup>4</sup> P. J. Chupas, M. F. Cirraolo, J. C. Hanson, and C. P. Grey, *J. Am. Chem. Soc.* **123**, 1694 (2001).
- <sup>5</sup> P. M. Woodward, *Acta Cryst.* **B53**, 32 (1997).
- <sup>6</sup> N. Troullier and J. L. Martins, *Phys. Rev. B* **43**, 1993 (1991).
- <sup>7</sup> P. Blaha, K. Schwarz, and J. Luitz, in *Proceedings of WIEN97* (Techn. Universität Wien, Austria, 1999).
- <sup>8</sup> D. J. Singh, *Planewaves, Pseudopotentials and the LAPW Method* (Kluwer Academic, Boston, 1994).
- <sup>9</sup> D. M. Ceperley and B. J. Alder, *Phys. Rev. Lett.*, **45**, 566, 1980.
- <sup>10</sup> S. H. Vosko, L. Wilk, and M. Nusair, *Can. J. Phys.*, **58**, 1200, 1980. L. Wilk and S. H. Vosko, *J. Phys. C Solid State*, **15**, 2139, 1982.
- <sup>11</sup> V. I. Zinenko and M. G. Zamkova, *Phys. Solid State* **42**, 1348 (2000).
- <sup>12</sup> O. V. Ivanov and E. G. Maksimov, *JETP* **81** 1008 (1995).
- <sup>13</sup> P. Danial, A. Bulou, M. Rousseau, J. Nouet, J. L. Fourquet, M. Leblanc, and R. Burriel, *J. Phys.: Condens. Matter* **2**, 5663 (1990).
- <sup>14</sup> P. Danial, A. Bulou, M. Rousseau, and J. Nouet, *Phys. Rev. B* **42**, 10545 (1990).
- <sup>15</sup> P. Yu and M. Cardona, *Fundamentals of Semiconductors*, second edition, page 251. (Springer, 1999)
- <sup>16</sup> B. Adolph, V. I. Gavrilenko, K. Tenelson, F. Bechstedt and R. Del Sole, *Phys. Rev. B* **53** 9797 (1996).
- <sup>17</sup> M. S. Hybertsen and S. G. Louie, *Phys. Rev. B* **35** 5585 (1987).
- <sup>18</sup> This was pointed out to us by P. Madden (private communication), and later also appeared in our charge contour plot.
- <sup>19</sup> L. Bernasconi, P. A. Madden and M. Wilson, *Phys. Chem. Comm.* **5**, 1 (2002).
- <sup>20</sup> R. Blinc and B. Žeks, *Soft Modes in Ferroelectrics and Antiferroelectrics*, edited by E. P. Wohlfarth (North-Holland Publishing Co. Amsterdam, 1974)
- <sup>21</sup> C. Kittel, *Introduction to Solid State Physics*, seventh edition, page 391 and references therein, John Wiley and Son, New York.